Transient acoustic processes in a low-Mach-number shear flow

By MENG WANG AND D. R. KASSOY

Department of Mechanical Engineering *and* Center for Combustion Research,
University of Colorado, Boulder, CO 80309, USA

A systematic perturbation procedure, based on a small mean flow Mach number and large duct Reynolds number, is employed to formulate and solve an initial-boundary-value problem for acoustic processes in a shear flow contained within a rigid-walled parallel duct. The results describe the general transient evolution of acoustic waves driven by a plane source located at a given duct cross-section. Forced bulk oscillations near the source and oblique wave generation are shown to result from refraction of the basic planar axial disturbance by the shear flow. Refraction also causes the axial waves to exhibit higher-order amplitude variations in the transverse direction. As the source frequency approaches certain critical values, specific refraction-induced oblique waves evolve into amplifying purely transverse waves. As a result, the magnitude of the refraction effect increases with time, and quasi-steady solutions do not exist. The analysis is extended to the thin acoustic boundary layer adjacent to the solid walls to examine the shear-layer structure induced by the variety of acoustic waves in the core flow. Nonlinear effects and acoustic streaming are shown to be negligibly small on the scale of a few axial wavelengths.

1. Introduction

The effect of shear flow on acoustic wave propagation was first studied analytically by Pridmore-Brown (1958), who derived the following linearized wave equation for propagation in a fully developed duct flow:

$$\frac{1}{c_0^2}p_{tt} = (1-M^2)\,p_{xx} + p_{yy} - \frac{2M}{c_0}p_{xt} + 2\rho_0\,c_0 M_y\,v_x, \tag{1}$$

where p and v are the acoustic pressure and normal velocity, respectively. The sound speed of the mean state (p_0, ρ_0, T_0) is c_0, and $M = M(y)$ is the shear-flow Mach number. Earlier efforts have been focused on seeking quasi-steady solutions of the type $p = F(y)\,e^{i(\kappa x - t)}$. Cross-stream eigenfunctions F and eigenvalues κ are obtained to describe the shear-flow distortion of specific propagating acoustic wave modes. Both asymptotic solutions (Pridmore-Brown 1958) and numerical solutions (Mungur & Gladwell 1969) demonstrate that for a downstream-propagating axial wave (the fundamental mode), the acoustic pressure at the wall is significantly larger than the value of the centreline. Calculations for upstream propagation (Hersh & Catton 1971) show a reversed trend of acoustic pressure distribution.

Quasi-steady theory is useful for describing only limited types of acoustic phenomena owing to the restrictive nature of the presumed solution form. For example, one cannot use it to track the evolution of an initial disturbance toward the

quasi-steady waveform, if it exists. Solutions describing temporal amplitude growth (resonance) are excluded entirely. Furthermore, the quasi-steady solution does not provide the absolute magnitude of a propagating wave and its relation to a specific acoustic source, nor does it include new waves that may be generated by refraction of the given wave. It is also important to note that the solution as well as the formulation exclude the acoustic boundary layer where the wave motion is damped by viscous effects to satisfy no-slip conditions on the duct wall. These limitations can be overcome by developing an initial-boundary-value solution for acoustic disturbances in a shear flow. In addition to the acoustic analysis one must consider viscous boundary-layer effects adjacent to the duct walls.

Previous oscillatory boundary-layer analyses are mostly for incompressible flows. For example, Stokes (1851) studied the long-time quasi-steady response of a viscous fluid to boundary oscillation; Sexl (1930) and Uchida (1956) investigated laminar pipe flow due to oscillatory pressure gradient. The heat transfer process in the pulsating pipe flow was examined by Romie (1956). These studies all demonstrate the velocity overshoot at the edge of the viscous layer, commonly known as Richardson's annular effect (Richardson & Tyler 1929). More recently, Barnett (1970, 1981) studied the pulsating pipe flow process based on linearized turbulent Navier–Stokes equations. Rott's (1980) investigation of acoustic oscillations in an infinite gas region parallel to a flat plate is more closely related to the present study, because he used a low-Mach-number compressible gas model. The effect of mean temperature variation along the direction of oscillation is included, but no mean flow is allowed.

In contrast to the traditional quasi-steady linear approach, Baum & Levine (1987) developed numerical solutions to an initial-boundary-value problem in order to describe uni-directional acoustic propagation in an axisymmetric cylinder with a coexisting mean shear flow. The code is based on Reynolds-averaged Navier–Stokes equations for compressible flow, coupled with the k–ϵ turbulence model. Acoustic disturbances, generated by a disk-shaped acoustic source of spatially uniform strength, are studied over a few acoustic wavelengths. In this short-time calculation one cannot expect to find the quasi-steady wave structure solution used to solve (1).

The present study is inspired by the limitations of the classical quasi-steady solutions mentioned above, and the lack of long-time results in Baum & Levine's work. The physical system under consideration involves a horizontal parallel duct containing a fully developed low-Mach-number shear flow (cf. figure 1), a two-dimensional duct counterpart to the cylinder considered by Baum & Levine (1987). An initial-boundary-value problem is formulated for an acoustic disturbance propagating into the imposed shear flow. The disturbance is initiated by a source located at a given duct cross-section. Such an approach ensures the spontaneous appearance of all types of acoustic waves, including non-axial waves, arising from the refraction of the basic axial wave, and provides an explicit relationship between the driving acoustic source and the evolving wave field.

The analysis is based on a laminar flow model for a viscous, heat-conducting fluid. By using a rational approximation procedure, in §2, transport effects are shown in a formal manner to be limited to extremely thin acoustic boundary layers adjacent to the duct wall. Perturbation methods, based on the small mean flow Mach-number parameter M, are employed to find solutions for both the transport-free core region in §3 and the viscous layer in §4. The solution procedure is especially simplified due to the low-Mach-number simplifications. Finally, in §5, the results are discussed in comparison with the numerical solutions of Baum & Levine (1987), and the major findings of the present work are summarized.
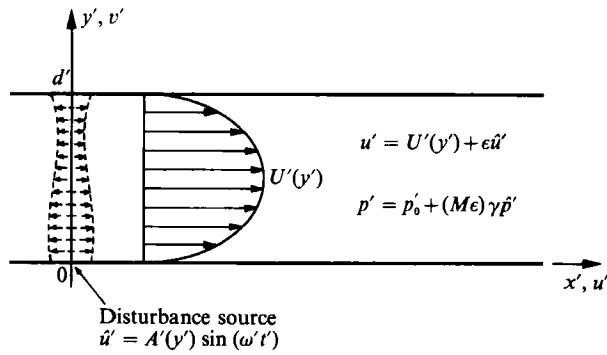
FIGURE 1. The physical system: source-generated acoustic oscillation in a fully developed duct flow.

The results demonstrate that refraction, known to distort the pressure distribution of the leading-order axial wave, is also the source of new and dispersive acoustic transients. When non-resonant conditions prevail, these transients evolve into oblique propagating waves and a forced bulk response at the acoustic source frequency. The former correspond to the selected higher modes of quasi-steady propagation in duct acoustics, while the bulk response is composed of an infinite number of attenuated modes that decay rapidly away from the plane acoustic source. The quasi-steady axial wave solution agrees with those from the classical studies (Pridmore-Brown 1958; Hersh & Catton 1971). Resonance occurs in one of the propagated modes if the duct width is some integer multiple of the driving acoustic wavelength. In this case purely transverse waves with growing amplitude are found to exist that cause a drastic increase in refraction effects.

In the viscous, heat-conducting acoustic boundary layers, a complex response arises from the variety of acoustic waves in the core. The transverse velocity in the acoustic boundary layer is much larger and more complicated than that predicted by Rott (1980), because it must match with the core solution that contains refraction effects. The refraction magnitude and the acoustic boundary-layer thickness obtained from the perturbation solutions are found to be comparable with those of Baum & Levine (1987).

2. Mathematical formulation

The complete dimensionless equations describing the compressible fluid motion in a planar duct shown in figure 1 can be written in the form

$$p = \rho T, \tag{2}$$

$$\rho_t + M[(\rho u)_x + (\rho v)_y] = 0, \tag{3}$$

$$\rho[u_t + M(u u_x + v u_y)] = -\frac{1}{\gamma M} p_x + \frac{M}{\Omega Re}(u_{yy} + \tfrac{4}{3}\Omega^2 u_{xx} + \tfrac{1}{3}\Omega^2 v_{xy}), \tag{4}$$

$$\rho[v_t + M(u v_x + v v_y)] = -\frac{1}{\gamma M \Omega^2} p_y + \frac{M}{\Omega Re}(\Omega^2 v_{xx} + \tfrac{4}{3}v_{yy} + \tfrac{1}{3}u_{xy}), \tag{5}$$

$$\rho[T_t + M(u T_x + v T_y)] = -M(\gamma-1)p(u_x + v_y) + \frac{M\gamma}{\Omega Pr Re}(T_{yy} + \Omega^2 T_{xx})$$

$$+ \frac{M^3}{\Omega Re}\gamma(\gamma-1)[(u_y + \Omega^2 v_x)^2 + 2\Omega^2(u_x^2 + v_y^2) - \tfrac{2}{3}\Omega^2(u_x + v_y)^2], \tag{6}$$

where for convenience the thermophysical properties are assumed constant. The non-dimensional variables are defined in terms of dimensional quantities by

$$
(p, \rho, T) = \frac{(p', \rho', T')}{(p_0', \rho_0', T_0')}, \quad u = \frac{u'}{U_c'}, \quad v = \frac{v'}{v_R'},
$$
$$
t = \frac{t'}{t_R'}, \quad x = \frac{x'}{x_R'}, \quad y = \frac{y'}{d'}.
\tag{7}
$$

Quantities p_0', ρ_0', and T_0' are thermodynamic properties of the gas at mean state, d' is the width of the duct and U_c' the characteristic velocity of the mean flow. The characteristic timescale is defined as the inverse of the circular frequency of the axial acoustic wave, $t_R' = 1/\omega'$, so that the wavelength gives the proper axial lengthscale $x_R' = c'/\omega'$. The characteristic transverse velocity $v_R' = M\omega' d'$. The dimensionless groups in (2)–(6) defined by

$$
M = \frac{U_c'}{c'}, \quad Re = \frac{U_c' d'}{\nu'}, \quad Pr = \frac{\nu'}{\alpha'}, \quad \Omega = \frac{\omega' d'}{c'},
\tag{8}
$$

are the maximum mean flow Mach number, the mean flow Reynolds number, the Prandtl number, and the normalized axial acoustic frequency, respectively. One notices that Ω is the ratio of the transverse acoustic time in the duct to the wave period.

In the present study solutions to the system described above are sought in the limit $1/Re \rightarrow 0$ and $M \rightarrow 0$, where it is assumed that $1/Re \ll M$. Additionally, one assumes that the Prandtl number is an order-one quantity and $\Omega \leqslant O(1)$.

As in previous studies (Pridmore-Brown 1958; Mungur & Gladwell 1969; Hersh & Catton 1971), the basic steady flow in the duct is assumed to be fully developed. It is driven by a pressure gradient which is inversely proportional to the Reynolds number of the flow. One can easily derive from (2)–(5) that

$$
u = U(y), \quad v = 0, \quad \mathrm{d}p/\mathrm{d}x = O(M^2/Re).
\tag{9}
$$

Obviously, on the lengthscale x_R' the variation of p is negligibly small.

Since the Reynolds number is very large, it is observed from (2)–(6) that, except for the extremely thin acoustic boundary layers adjacent to the solid surfaces which will be discussed in detail in §4, the wave motion in the core region is basically unaffected by transport effects. In this limiting case, the state, continuity and energy equations (cf. (2), (3) and (6)) can be combined to give the familiar results

$$
p = \rho^\gamma + O\left(\frac{M}{\Omega Re}\right), \quad T = \rho^{\gamma-1} + O\left(\frac{M}{\Omega Re}\right).
\tag{10}
$$

These isentropic relations, together with the inviscid versions of (3)–(5), suffice to describe the acoustic wave motion in the core.

When the fully developed duct flow is disturbed by an $O(\epsilon)$ acoustic velocity,

$$
u = U(y) + \epsilon \hat{u}, \quad v = \epsilon \hat{v},
\tag{11}
$$

it can be shown that the thermodynamic corrections are always $O(M\epsilon)$, in order to balance the acoustic components in the governing equations (3)–(5). Accordingly, p, ρ and T are put into the following form:

$$
p = 1 + (M\epsilon)\gamma\hat{p}, \quad \rho = 1 + (M\epsilon)\hat{\rho}, \quad T = 1 + (M\epsilon)\hat{T}.
\tag{12}
$$

The continuity equation (3) can be rewritten in terms of acoustic variables as

$$
\hat{\rho}_t + \hat{u}_x + \hat{v}_y + MU(y_x)\hat{\rho}_x + (M\epsilon)\left[(\hat{\rho}\hat{u})_x + (\hat{\rho}\hat{v})_y\right] = 0.
\tag{13}
$$

Similarly, the x and y momentum equations become

$$\hat{u}_t + M[U(y)\,\hat{u}_x + \hat{v}U'(y)] + (M\epsilon)(\hat{u}\hat{u}_x + \hat{v}\hat{u}_y) = -\frac{\hat{p}_x}{1 + (M\epsilon)\hat{\rho}}, \tag{14}$$

$$\hat{v}_t + MU(y)\,\hat{v}_x + (M\epsilon)(\hat{u}\hat{v}_x + \hat{v}\hat{v}_y) = -\frac{\hat{p}_y}{\Omega^2[1 + (M\epsilon)\hat{\rho}]}. \tag{15}$$

In (13)–(15) terms containing $U(y)$ represent the shear-flow interaction with the acoustic field. They are $O(M)$ quantities. The nonlinear product terms are of $O(\epsilon M)$. There are three interesting asymptotic limits that can be applied to (13)–(15) for low-Mach-number shear flows:

(i) *The parameters satisfy the inequality $\epsilon \ll M \ll 1$, and the asymptotic limit $\epsilon \to 0$, M fixed is used.* The nonlinear terms can be ignored since their magnitudes are small relative to M. A combination of (13), (14) and (15) generates a leading-order acoustic equation equivalent to (1). This demonstrates that the previous quasi-steady analyses by Pridmore-Brown (1958), Mungur & Gladwell (1969), and Hersh & Catton (1971) are asymptotically accurate for extremely small-amplitude acoustics relative to the characteristic shear-flow Mach number.

(ii) *The parameters satisfy the inequality $O(\epsilon) = M \ll 1$, and the asymptotic limit $M \to 0$ is used.* If $O(M^2)$ terms in (13)–(15) are uniformly ignored relative to $O(M)$ terms in the asymptotic limit, their analogue to (1) contains no $O(M^2)$ term. This shows that the Pridmore-Brown results are formally valid to $O(M)$ where $M \ll 1$. Numerical studies by Baum & Levine (1987) are primarily concerned with this regime.

(iii) *The parameters satisfy the inequality $M \ll \epsilon \leqslant O(1)$, and the asymptotic limit $M \to 0$, ϵ fixed is used.* An examination of (13)–(15) shows that the nonlinear terms and the refraction-producing terms containing $U(y)$ are of the same magnitude, $O(M)$, in the limit. As a result, (1) which is purely linear cannot describe acoustic phenomena when the pressure disturbance in (12) is $O(M)$.

The following analysis is focused formally on Case (ii) described above, although the solutions for acoustic variables are equally valid for Case (i) since both cases yield identical truncated versions of (13)–(15) to $O(M)$. The initial state of the disturbance quantities is described by

$$t = 0, \quad \hat{u} = \hat{v} = \hat{p} = 0. \tag{16}$$

Acoustic waves are excited at $x = 0$ by imposing a periodic horizontal disturbance velocity

$$x = 0, \quad \hat{u} = A\sin(t), \tag{17}$$

where the amplitude A is in general y-dependent, although the simpler case of constant amplitude is emphasized here. The normal velocity component generated in the viscous acoustic boundary layer is of much smaller magnitude relative to the core flow magnitude, as will be shown later. Hence, so far as the acoustic core region is concerned, the impermeable condition

$$y = 0, 1; \quad \hat{v} = 0 \tag{18}$$

can be applied directly to describe the acoustic behaviour close to the duct walls.

3. Core solution

3.1. *Acoustic transients due to axial wave refraction*

First, the acoustic quantities are expanded asymptotically in terms of M in the following manner:

$$\hat{\Psi} = \Psi_1 + M\Psi_2 + O(M^2), \quad \Psi = (u, v, p, \rho, T). \tag{19}$$

In order to account for the small changes in the absolute wave propagation speed due to the $O(M)$ mean flow, it is necessary to use a strained coordinate

$$\bar{x} = \frac{x}{1 + M\tilde{U}_0 + \dots}, \tag{20}$$

where

$$\tilde{U}_0 = \int_0^1 U(y)\,\mathrm{d}y \tag{21}$$

is the bulk shear flow velocity area-averaged across the duct. One finds from (13)–(15) ordered sets of equations:

$$\rho_{1t} + u_{1\bar{x}} + v_{1y} = 0, \tag{22}$$

$$u_{1t} + p_{1\bar{x}} = 0, \tag{23}$$

$$v_{1t} + \frac{1}{\Omega^2} p_{1y} = 0, \tag{24}$$

and

$$\rho_{2t} + u_{2\bar{x}} + v_{2y} = -U(y)\,\rho_{1\bar{x}} + \tilde{U}_0 u_{1\bar{x}}, \tag{25}$$

$$u_{2t} + p_{2\bar{x}} = \tilde{U}_0\,p_{1\bar{x}} - U(y)\,u_{1\bar{x}} - U'(y)\,v_1, \tag{26}$$

$$v_{2t} + \frac{1}{\Omega^2} p_{2y} = -U(y)\,v_{1\bar{x}}. \tag{27}$$

Additionally, the isentropic relations (10) imply that

$$p_1 = \rho_1, \quad p_2 = \rho_2. \tag{28}$$

Equations (22)–(24) are combined to generate the linear, homogeneous wave equation for p_1,

$$p_{1tt} - \left(p_{1\bar{x}\bar{x}} + \frac{1}{\Omega^2} p_{1yy} \right) = 0. \tag{29}$$

The leading-order acoustic equation is seen to be unaffected by the mean shear flow, except for the bulk convection effect incorporated into the variable $\bar{x}$. If the boundary velocity oscillation has a constant amplitude, $A = 1$ in (17), the solution satisfying (16)–(18) describes a wave train propagating axially into a quiescent gas,

$$p_1 = u_1 = \sin(t - \bar{x}), \quad v_1 = 0. \tag{30}$$

Note that ahead of the wavefront, when $\bar{x} \geqslant t$, all the acoustic quantities are zero.

In order to study the explicit effect of the shear-flow velocity gradient on the acoustic field, (25)–(27) are combined to give the second-order analogue of (29),

$$p_{2tt} - \left(p_{2\bar{x}\bar{x}} + \frac{1}{\Omega^2} p_{2yy} \right) = -2\tilde{U}_0\,p_{1\bar{x}\bar{x}} - 2U(y)\,p_{1\bar{x}t} + 2U'(y)\,v_{1\bar{x}}. \tag{31}$$

The forcing function, representing the interactions between the shear flow and the leading-order acoustics, is simplified for the case considered here, i.e. when the boundary oscillation is y-independent. Upon inserting (30) into (31), the latter can be rewritten as

$$p_{2tt} - \left(p_{2\bar{x}\bar{x}} + \frac{1}{\Omega^2} p_{2yy} \right) = -2[U(y) - \tilde{U}_0]\sin(t - \bar{x}) \tag{32}$$

for $\bar{x} \leqslant t$. The initial and boundary conditions necessary to solve (32) are derived by an appropriate combination of the preceding results in this section with (16)–(18). They are given by

$$t = 0, \quad p_2 = p_{2t} = 0; \tag{33}$$

$$\bar{x} = 0, \quad p_{2\bar{x}} = [U(y) - \tilde{U}_0]\cos(t); \quad \bar{x} \to \infty, \quad p_2 = \text{finite}; \tag{34}$$

$$y = 0;1, \quad p_{2y} = 0. \tag{35}$$

The hyperbolic equation system (32)–(35) can be solved by a combination of Laplace transform and Fourier series methods, as outlined below. If Q and s are used to denote the transformed variables of p_2 and t, respectively, a Laplace transform of (32)–(35) with respect to time t yields

$$Q_{\bar{x}\bar{x}} + \frac{1}{\Omega^2} Q_{yy} - s^2 Q = 2 [U(y) - \tilde{U}_0] \frac{e^{-s\bar{x}}}{1+s^2}; \tag{36}$$

$$\bar{x} = 0, \quad Q_{\bar{x}} = [U(y) - \tilde{U}_0] \frac{s}{s^2+1}; \qquad \bar{x} \to \infty, \quad Q = \text{finite}; \tag{37}$$

$$y = 0; 1, \quad Q_y = 0. \tag{38}$$

The homogeneous boundary condition (38) suggests that a Fourier series solution of the form

$$Q = a_0(\bar{x}, s) + \sum_{n=1}^{\infty} a_n(\bar{x}, s) \cos(n\pi y) \tag{39}$$

is obtainable. Once the shear-flow velocity $U(y)$ is Fourier decomposed into

$$U(y) = \tilde{U}_0 + \sum_{n=1}^{\infty} \tilde{U}_n \cos(n\pi y), \tag{40}$$

where the bulk part $\tilde{U}_0$ is given by (21), and

$$\tilde{U}_n = 2 \int_0^1 U(y) \cos(n\pi y) \, dy, \tag{41}$$

it becomes clear immediately from (36)–(38) that $a_0 = 0$. The nth Fourier coefficient, for $n = 1, 2, \ldots$, is governed by

$$a_n'' - (s^2 + q_n^2) a_n = 2\tilde{U}_n \frac{e^{-s\bar{x}}}{1+s^2}, \tag{42}$$

where the parameter q_n is defined as

$$q_n = n\pi/\Omega. \tag{43}$$

The solution to (42), which satisfies

$$a_n'(0) = \tilde{U}_n \frac{s}{s^2+1} \tag{44}$$

and has a finite value as $\bar{x} \to \infty$, is obtained as

$$a_n = \tilde{U}_n \left(\frac{2}{q_n^2} - 1 \right) \frac{s}{s^2+1} \frac{\exp[-(s^2+q_n^2)^{\frac{1}{2}} \bar{x}]}{(s^2+q_n^2)^{\frac{1}{2}}} - \frac{2\tilde{U}_n}{q_n^2} \frac{e^{-s\bar{x}}}{1+s^2}. \tag{45}$$

Upon using (45) in (39), and taking the inverse Laplace transform by means of an extended Laplace transform table (Oberhettinger & Badii 1973) and the convolution theorem, one finally obtains

$$p_2 = -\sin(t-\bar{x}) \sum_{k=1}^{\infty} \frac{2\tilde{U}_k}{q_k^2} \cos(k\pi y)$$

$$+ \sum_{n=1}^{\infty} \tilde{U}_n \left(\frac{2}{q_n^2} - 1 \right) \int_{\bar{x}}^{t} \cos(t-\xi) J_0[q_n(\xi^2 - \bar{x}^2)^{\frac{1}{2}}] \, d\xi \cos(n\pi y), \tag{46}$$

where J_0 is the zeroth-order Bessel function of the first kind.

The first term on the right-hand side of (46) represents a quasi-steady, axial travelling wave (fundamental duct mode), with y-dependent amplitude given by the summation. It is an $O(M)$ correction to the leading-order axial wave (cf. (30)) and thus describes the effect of shear-flow-induced refraction on the propagating axial wave. As predicted by the classical theory, the axial wave acoustic pressure redistributes itself non-uniformly across the duct. The y-dependent amplitude function grows rapidly with driving acoustic frequency (cf. (46) and (43)) and varies with shear flow velocity profile. It is, within a constant, equivalent to the result of Hersh & Catton's (1971) perturbation study, if the latter is rewritten in Fourier decomposed form. However, here the amplitude is completely defined because the solution is obtained from an initial-boundary-value problem.

A second fundamental advantage of studying linear acoustic refraction phenomena in terms of an initial-boundary-value problem is that the transient (non-quasi-steady) evolution of the acoustic refraction and its absolute magnitude can be found explicitly, a result not available from the classical studies (Pridmore-Brown 1958; Mungur & Gladwell 1969; Hersh & Catton 1971). The complete second term in (46) represents acoustic transients initiated by the passage of the leading-order axial wave through the shear flow, including dispersive effects. The transients evolve into oblique waves (higher propagated modes) and forced bulk vibration consisting of infinite numbers of attenuated modes, as will be shown in the next subsection.

The $O(M)$ axial and transverse acoustic velocities can be obtained by integrating (26) and (27), respectively. They are

$$u_2 = -\sin{(t-\bar{x})} \sum_{k=1}^{\infty} \left(\frac{2}{q_k^2} - 1\right) \tilde{U}_k \cos{(k\pi y)} + \sum_{n=1}^{\infty} \tilde{U}_n \left(\frac{2}{q_n^2} - 1\right) \bar{x} h_n(t, \bar{x}) \cos{(n\pi y)}, \quad (47)$$

$$h_n = \int_{\bar{x}}^{t} \frac{J_0[q_n(\zeta^2 - \bar{x}^2)^{\frac{1}{2}}]}{\zeta} \, d\zeta - \int_{\bar{x}}^{t} \int_{\bar{x}}^{\zeta} \left[\frac{\sin{(\zeta-\xi)}}{\xi} - \frac{\cos{(\zeta-\xi)}}{\xi^2}\right] J_0[q_n(\xi^2 - \bar{x}^2)^{\frac{1}{2}}] \, d\xi \, d\zeta, \quad (48)$$

$$v_2 = [\cos{(t-\bar{x})} - 1] \sum_{k=1}^{\infty} \frac{2\tilde{U}_k}{k\pi} \sin{(k\pi y)}$$

$$+ \sum_{n=1}^{\infty} \frac{2\tilde{U}_n}{n\pi} (1 - \tfrac{1}{2}q_n^2) \int_{\bar{x}}^{t} \int_{\bar{x}}^{\zeta} \cos{(\zeta-\xi)} J_0[q_n(\xi^2 - \bar{x}^2)^{\frac{1}{2}}] \, d\zeta \sin{(n\pi y)}. \quad (49)$$

The two terms in both the u_2 and v_2 expressions again represent the quasi-steady axial wave and other transient phenomena, corresponding to those in (46). For large $\bar{x}$, one can show from (48) that $h_n \sim O(\bar{x}^{-1})$, so that u_2 remains bounded despite the explicit $\bar{x}$ proportionality.

3.2. *The evolution to quasi-steady propagation*

Insightful results for the long-time properties of p_2 can be obtained from the asymptotic properties of the integral

$$I_n(t, \bar{x}) = \int_{\bar{x}}^{t} \cos{(t-\xi)} J_0[q_n(\xi^2 - \bar{x}^2)^{\frac{1}{2}}] \, d\xi. \quad (50)$$

When $q_n \neq 1$, (50) converges for large values of t such that

$$\lim_{t \to \infty} I_n = \begin{cases} \dfrac{\cos{(t)} \exp{[-\bar{x}(q_n^2 - 1)^{\frac{1}{2}}]}}{(q_n^2 - 1)^{\frac{1}{2}}}, & q_n > 1 \\ \dfrac{\sin{[t - (1 - q_n^2)^{\frac{1}{2}}\bar{x}]}}{(1 - q_n^2)^{\frac{1}{2}}}, & q_n < 1, \end{cases} \quad (51)$$
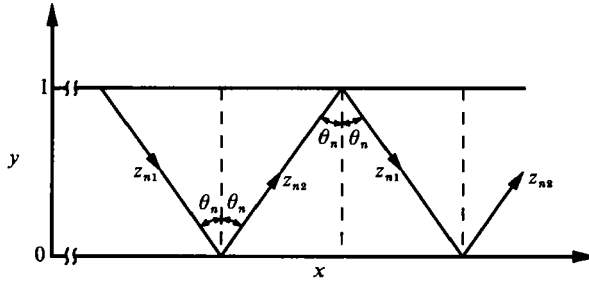
FIGURE 2. The path of an oblique travelling wave, represented by (53) and (54).

when $\bar{x} = O(1)$ (Gradshteyn & Ryzhik 1980). It follows from (46) and (51) that the non-resonant long-time solution for the refractive acoustic pressure can be written as

$$
p_2 = -\sin{(t-\bar{x})} \sum_{k=1}^{\infty} \frac{2\tilde{U}_k}{q_k^2} \cos{(k\pi y)}
$$

$$
+ \sum_{n=1}^{N} \tilde{U}_n \left(\frac{2}{q_n^2} - 1\right) \frac{\sin{[t - (1 - q_n^2)^{\frac{1}{2}} \bar{x}]}}{(1 - q_n^2)^{\frac{1}{2}}} \cos{(n\pi y)}
$$

$$
+ \cos{(t)} \sum_{n=N+1}^{\infty} \tilde{U}_n \left(\frac{2}{q_n^2} - 1\right) \frac{\exp{[-(q_n^2 - 1)^{\frac{1}{2}} \bar{x}]}}{(q_n^2 - 1)^{\frac{1}{2}}} \cos{(n\pi y)}, \tag{52}
$$

where N is defined such that $q_N < 1 < q_{N+1}$.

The second full term in (52) contains N Fourier modes, or higher propagated modes in classical acoustics terms. Each mode can be rewritten as a pair of oblique travelling waves. This is illustrated by rewriting the nth mode, denoted by P_n, as

$$
P_n = \frac{\tilde{U}_n(2 - q_n^2)}{2q_n^2(1 - q_n^2)^{\frac{1}{2}}} [\sin{(t - z_{n1})} + \sin{(t - z_{n2})}], \tag{53}
$$

where

$$
z_{n1} = (1 - q_n^2)^{\frac{1}{2}} \bar{x} - n\pi y, \quad z_{n2} = (1 - q_n^2)^{\frac{1}{2}} \bar{x} + n\pi y \tag{54}
$$

represent a pair of oblique paths for the travelling waves, shown in figure 2. The wave reflects repeatedly from both duct walls as it travels along. Upon each reflection, it switches from one path to the other. If the transverse coordinate is rescaled by $Y = \Omega y$, so that both Y are x and normalized using the same characteristic length-scale $x'_R = c'/\omega'$, one easily finds that the phase speed of the nth mode along the z_{n1}, z_{n2} paths is unity, while the phase speed along the x-axis varies from 0 to ∞, depending on the angle of incidence $\theta_n = \sin^{-1}[(1 - q_n^2)^{\frac{1}{2}}]$. The latter is identical to the angle of reflection because of the rigid-wall assumption. Note that when q_n is close to 1, one pair of large-amplitude oblique waves become nearly transverse, so that a form of wave trapping appears. This type of result, to be discussed in full in §3.3, implies that a resonance occurs when $q_n \to 1^-$ and amplitude growth with time can be expected.

The oblique travelling waves exist only when $q_n < 1$. In dimensional terms, this implies that $n < 2d'/\lambda'$ (λ' is the wavelength) must be satisfied in order for the waves to propagate. The number of non-axial travelling wave modes is thus proportional
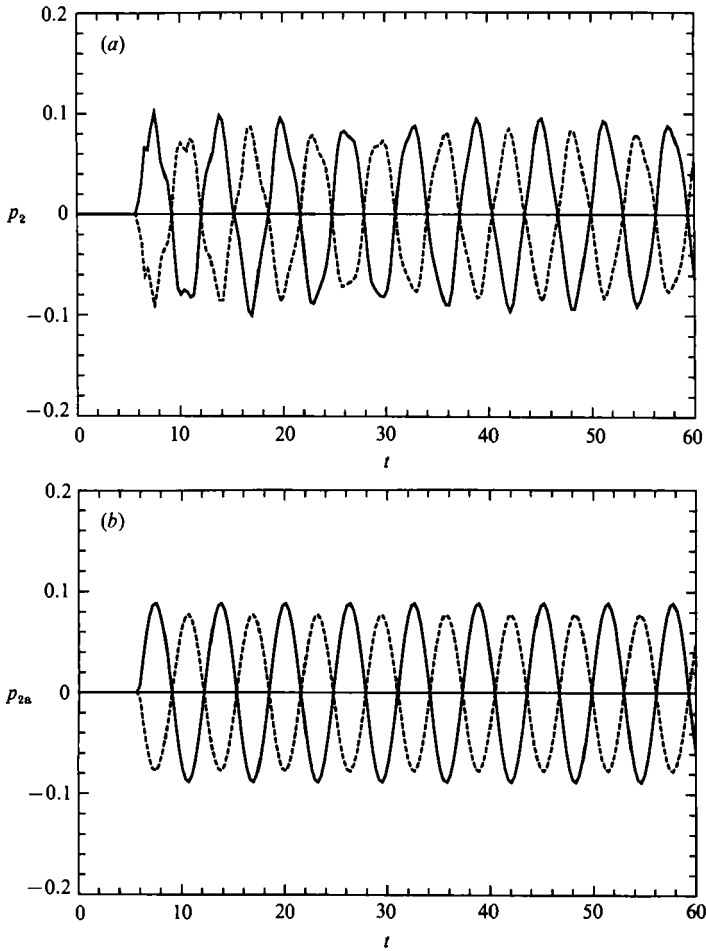
FIGURE 3. Time variations of (a) the second-order acoustic pressure p_2; (b) its axial wave contribution p_{2a} at $x = 2\pi$, $y = 0$ (———) and $\frac{1}{2}$ (- - - -), as calculated from (46). The total acoustic pressure $\hat{p} = p_1 + M p_2$ for the wave field generated by the plane source disturbance $u(x = 0) = \sin(t)$ in the laminar duct flow $U = 4y(1-y)$. The dimensionless frequency $\Omega = 2$, and the maximum mean flow Mach number $M = 0.1$.

to the duct width and inversely proportional to the acoustic wavelength. This is well known in quasi-steady duct acoustics (see, for example, Morse & Ingard 1968). However, the present transient analysis demonstrates explicitly that refraction of a basically axial wave is the direct source of the oblique propagating waves. These oblique waves will also interact with the shear flow as they propagate along, to generate more complex refraction effects. The latter are not included in the p_2 solution because they are $O(M)$ smaller.

The last term in (52) describes a bulk response of the gas, driven at the frequency of the acoustic source. These so-called attenuated modes ($q_n > 1$) decay exponentially along the x-axis, and thus normally affect only a small region close to the surface of the acoustic source. The penetration depth is proportional to $(q_n^2 - 1)^{-\frac{1}{2}}$. Given (43), one finds that small mode number n and high frequency Ω lead to deeper penetration. Resonance can also be viewed as occurring in the limit $q_n \to 1^+$, so that the first attenuated mode in (52) penetrates asymptotically far into the field, up to the basic
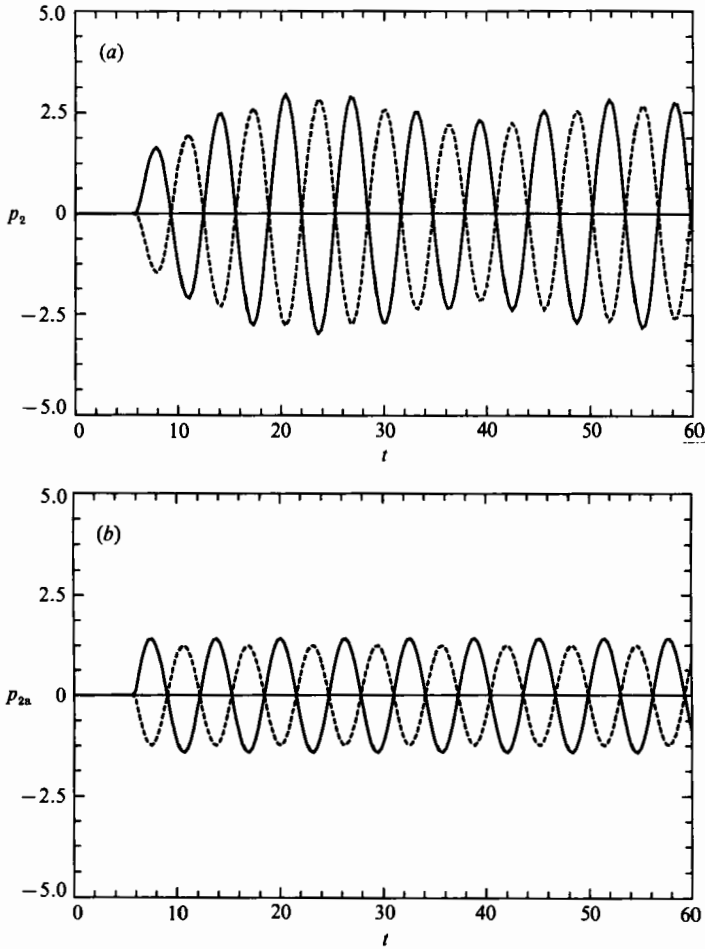
FIGURE 4. Time variations of (a) the second-order acoustic pressure p_2; (b) its axial wave contribution p_{2a} at $x = 2\pi$, $y = 0$ (——) and $\frac{1}{2}$ (- - - - -), when the dimensionless frequency $\Omega = 8$. Other conditions are identical to those in figure 3.

axial wavefront. In practical terms, only the first few attenuated modes from the second infinite summation are needed, because of the rapid decay of the Fourier coefficients with the mode number n.

The transition to the quasi-steady solution (52) can be illustrated by numerically evaluating the second-order acoustic pressure from the general formula (46). Since the Fourier series converges fairly rapidly, only the first 20 terms are used in each summation. A comparison of the results with those from summations of 40 or more terms shows agreement to within three decimal places. The integral I_n is computed by calling the QDAG integration subroutine from the IMSL software library, which uses a globally adaptive scheme based on Gauss–Kronrod rules. Representative examples of results for various acoustic frequencies and different types of duct mean flows are discussed below.

Figures 3 and 4 show the acoustic refraction effect in a fully developed laminar duct flow, described by $U = 4y(1-y)$. In figures 3(a) and 4(a), the time variations of p_2, evaluated from (46), are plotted for the cases of $\Omega = 2$ and 8 respectively, on a duct cross-section located at $x = 2\pi$, one wavelength downstream from the plane
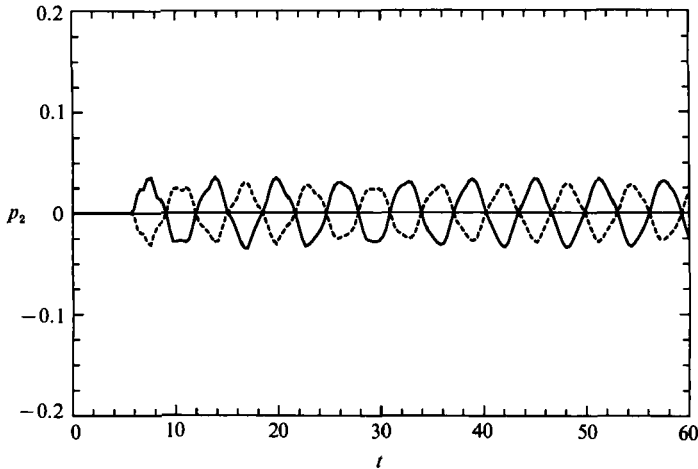
FIGURE 5. Time variations of the second-order acoustic pressure p_2 in a 'turbulent' mean flow field emulated by $U = (1-|2y-1|)^{\frac{1}{7}}$ at $x = 2\pi$, $y = 0$ (———) and $\frac{1}{2}$ (----). Other plotting conditions are identical to those in figure 3(a).

acoustic source. The solid lines represent the second-order acoustic pressures at the wall, while the dashed lines denote those at the centreplane of the duct. For comparison the axial wave contribution to p_2 (the first term in (46), henceforth denoted as p_{2a}) corresponding to the conditions in figures 3(a) and 4(a) are depicted in figures 3(b) and 4(b), respectively. The mean flow Mach number employed in the calculations is 0.1.

Since the mean flow is symmetric with respect to the duct centreplane, the Fourier coefficient $\tilde{U}_n = 0$ for n odd (cf. (41)). Thus the first oblique wave pair for p_2 corresponds to the $n = 2$ mode, whose cutoff frequency $\Omega = 2\pi$ ($\lambda' = d'$ in dimensional terms). The driving acoustic frequency is below the cutoff frequency for the $n = 2$ mode in figure 3, so that only the propagating axial wave exists in the quasi-steady state. The p_2 curves are thus similar to those for p_{2a}. The small discrepancy, caused by the acoustic transients induced in the gas medium when the wavefront first passes the given location, is seen to die out gradually as the solution converges to the quasi-steady solution (52). The effect of attenuated modes is negligibly small at $x = 2\pi$. Calculations conducted at other frequencies where there are no oblique waves show that the transient phenomenon is more prominent and disappears more slowly for lower-frequency cases then for higher-frequency cases.

The situation depicted in figure 4 is quite different. Here $\Omega = 8$, higher than the cutoff frequency for the $n = 2$ mode. The second-order acoustic pressure shown in figure 4(a) is a superposition of both the axial wave and one oblique wave pair, in addition to the small transient effect. As a result it is dramatically different, both in amplitude and phase, from the pure axial wave solution presented in figure 4(b).

Figure 5 depicts the time variation of p_2 in a 'turbulent' mean flow field emulated by $U = (1-|2y-1|)^{\frac{1}{7}}$. The other plotting conditions are identical to those used in producing figure 3(a), the laminar flow counterpart of figure 5. The refraction-induced acoustic pressure is observed to be much smaller in amplitude in the latter, because the mean flow represented by the one-seventh power law has a relatively small velocity gradient in most part of the duct. The high-velocity-gradient regions, concentrated near the two duct walls, are too narrow to promote acoustic refraction on a global scale.
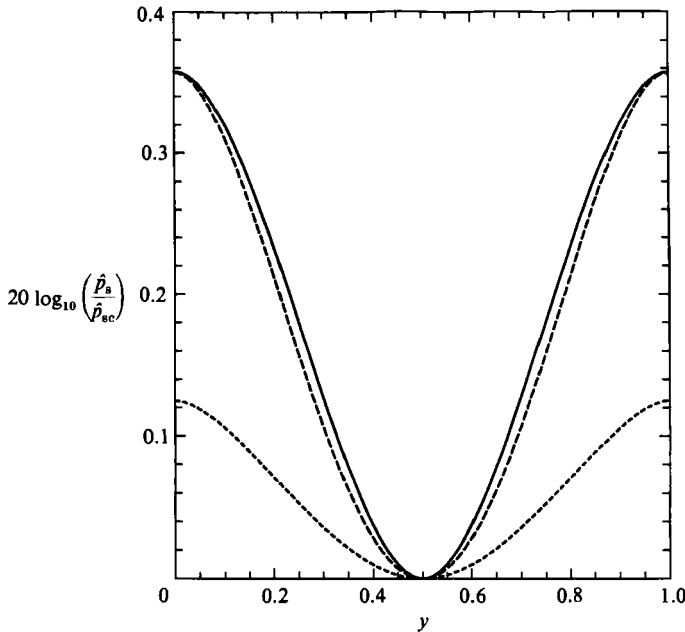
FIGURE 6. Axial wave quasi-steady acoustic pressure profile (in decibels) across the duct, for three types of shear flow: ——, $U = 1-|2y-1|$; ---, $U = 4y(1-y)$; ····, $U = (1-|2y-1|)^{\frac{1}{7}}$. The maximum shear flow Mach number $M = 0.1$, and the acoustic frequency $\Omega = \pi$.

The bulk convection of the acoustic wave by the mean flow can also be observed from figures 3–5. The wavefront emitted from the plane acoustic source arrives at $x = 2\pi$ after approximately 5.9 dimensionless time units, which is less than 2π, the time required for a wave to travel the same distance in a static medium.

The pressure curves in figures 3 and 5 suggest that a simple relation exists for quasi-steady acoustic refraction at relatively low driving frequency. If $\Omega < 2\pi$, so that non-axial waves are absent from (52), and if one is sufficiently far away from the plane acoustic source, where the effect of the attenuated modes is negligible, the entire quasi-steady solution contains axial waves only (cf. (19), (30) and (52)). In this case the total acoustic pressure normalized by its value at the duct centreplane provides a quantitative measure of the global refraction effect:

$$\frac{\hat{p}_{s}}{\hat{p}_{sc}} \approx 1 + M \sum_{k=1}^{\infty} \frac{2\tilde{U}_{k}}{q_{k}^{2}}[\cos\left(\tfrac{1}{2}k\pi\right) - \cos\left(k\pi y\right)], \tag{55}$$

where the subscripts s and c denote quasi-steady state and centreplane respectively. Equation (55) is in fact the ratio of the amplitude functions for the fundamental mode, equivalent to those found in earlier studies (Pridmore-Brown 1958; Mungur & Gladwell 1969; Hersh & Catton 1971) in the low-frequency range.

In figure 6 (55) is plotted for the case $\Omega = \pi$ and $M = 0.1$, for three types of mean flow conditions: $U = 1-|2y-1|$, $U = 4y(1-y)$, and $U = (1-|2y-1|)^{\frac{1}{7}}$. The familiar results are presented in decibels to follow convention. Obviously, the acoustic energy of the downstream-propagating axial wave train is channelled towards the walls. The linear and parabolic mean flows cause acoustic refraction effects of similar magnitudes, while the shear flow represented by the one-seventh power law generates the smallest refraction for the reason explained previously.

It must be emphasized that (55) or curves like those in figure 6 are accurate
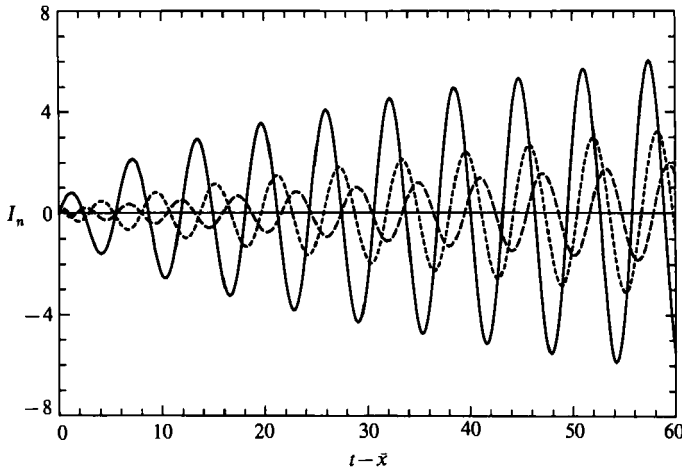
FIGURE 7. Numerical values of the integral (50) when $q_n = 1$, at three different $\bar{x}$-locations:
———, $\bar{x} = 0$; ———, 2π; ---- 4π.

representations of acoustic refraction phenomena in quasi-steady state, when the duct geometry only allows purely axial wave propagation for the given driving acoustic frequency. For $\Omega > 2\pi$, like the case depicted in figure 4, refraction of the planar axial wave also generates oblique travelling waves. The ratio of local acoustic pressure to that at the centreplane is both t- and x-dependent, and is not a useful representation of the transverse variation of the refraction effect.

3.3. *Resonant amplification of refraction phenomena*

The above discussions have been focused on non-resonant situations. The refractive pressure responses is dramatically different if $q_{n^*} = 1$, or in physical terms, $d' = \frac{1}{2}n^*\lambda'$, where n^* denotes the resonant mode. The resonance occurs because the frequencies of $J_0(\xi)$ and the harmonic function in (50) are nearly identical for $\xi \gg 1$ when $q_{n^*} = 1$. As a result, the integral becomes unbounded when $t \to \infty$, and no quasi-steady solutions exist. When the time is large, $\bar{x} \leqslant O(1)$, one can show that

$$I_{n^*}(t \gg 1, \bar{x}) \sim (2t/\pi)^{\frac{1}{2}} \cos{(t - \tfrac{1}{4}\pi)}. \tag{56}$$

In particular, at $\bar{x} = 0$ (50) can be evaluated exactly (Gradshteyn & Ryzhik 1980) to give

$$I_{n^*}(t, 0) = \int_0^t \cos{(t - \xi)} J_0(\xi) \, \mathrm{d}\xi = t J_0(t), \tag{57}$$

which agrees with (56) if the asymptotic property of J_0 for large t is used. By using (56) the resonant Fourier mode in (46) can be written asymptotically as

$$P_{n^*}(t \gg 1, \bar{x}) \sim \tilde{U}_{n^*} (t/2\pi)^{\frac{1}{2}} [\cos{(t - \Omega y - \tfrac{1}{4}\pi)} + \cos{(t + \Omega y - \tfrac{1}{4}\pi)}]. \tag{58}$$

It shows clearly the pair of purely transverse waves trapped in the duct with growing amplitudes.

Numerical evaluations of (50) for $q_n = 1$ are shown in figure 7, where the horizontal coordinate is the characteristic coordinate $t - \bar{x}$ for easier comparison. As the $\bar{x}$-value is increased, similar trends of growth with t are observed. However, the solutions at $t = 60$ still exhibit strong x-dependence because the asymptotic results described by (56) have yet to be reached.
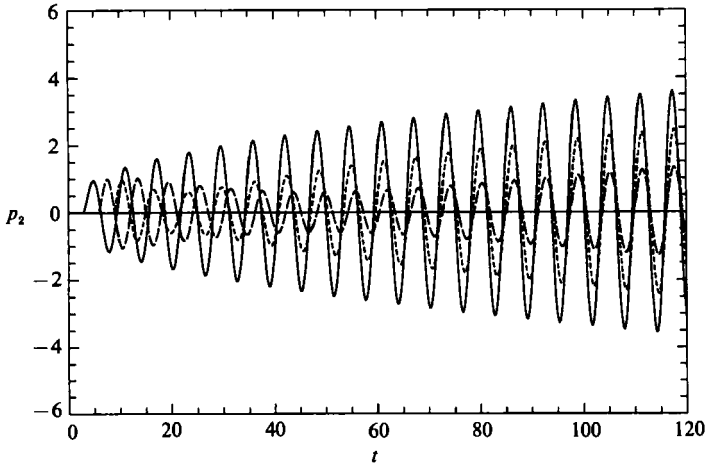
FIGURE 8. Time variations of the second-order acoustic pressure p_2 on the duct wall $y = 0$, at three axial locations (———, $x = \pi$; – – –, 2π; - - - - 3π), at resonant frequency $\Omega = 2\pi$. Other conditions are identical to those in figure 3 (a).

The effect of resonance on acoustic refraction is explicitly demonstrated in figure 8, where the variations of p_2 on the duct wall $y = 0$, at three separate axial locations, are plotted against time. The shear-flow profile is parabolic as used earlier. The driving frequency $\Omega = 2\pi$, so that the $n = 2$ mode in the second term of (46) is resonant. All the pressure curves show growth in amplitude after sufficient time elapses, when the growing resonant mode embedded in the second summation dominates the system in (46). For relatively short time, however, the resonant mode amplitude is not large compared with that of the fundamental mode (the entire first term in (46)). The amplitude of p_2 may initially decrease with time, as in the cases for $\bar{x} = 2\pi$ and 3π, owing to destructive interference.

Calculations for Ω-values slightly below and above the resonant frequency 2π show similar trends of growth for p_2. However, the amplitudes eventually approach large but finite limiting values predicted by (52).

The resonant result illustrates a fascinating mechanism for exciting and amplifying purely transverse waves in the duct through axial wave–shear flow interaction. This shows yet another distinct advantage of the present analytically based initial-boundary-value study. Numerical investigations for travelling wave refraction (Baum & Levine 1987) are limited to a few wave cycles only, owing to difficulties associated with non-reflective outflow boundary conditions. The results in figure 8 show that short-time solution behaviour cannot be used to determine if resonant amplifications of refractive pressure are occurring. The classical quasi-steady solutions (e.g. Pridmore-Brown 1958), on the other hand, cannot describe the resonant mode at all.

Owing to the $t^{\frac{1}{2}}$ growth of the resonant or near-resonant mode in p_2, one concludes that for such systems the perturbation expansion (19) breaks down as $t \sim O(M^{-2})$. A new derivation will be needed to predict its long-time behaviour, which will contain the resonance-enhanced refraction effects (the transverse waves) in the leading order.

It should also be noted that the validity of the perturbation solutions developed above depends on the value of Ω. In general, once the dimensionless frequency Ω becomes as large as $O(M^{-\frac{1}{2}})$, the magnitude of Mp_2 becomes comparable with that of p_1 (cf. (30), (46) and (43)), causing the breakdown of the asymptotic expansion (19).

The actual size of Mp_2 nevertheless also depends upon the magnitude of $\tilde{U}_n$. For mean duct flows symmetric with respect to the centreplane $y = \frac{1}{2}$, the largest terms in the Fourier summations in (46) and (52) vanish because $\tilde{U}_n = 0$ for n odd. As shown in the example calculations, p_2 remains $O(1)$ when the value of Ω is as large as 8.

In the high-frequency limit $\Omega \gg 1$, when acoustic refraction effects are no longer small correction terms of $O(M)$, a new theory needs to be developed which includes refraction in the leading-order acoustics.

3.4. *Acoustic transients due to a y-dependent boundary disturbance*

In this section non-axial acoustic transients generated by source oscillations with y-dependent amplitude is discussed.

If the velocity oscillation at the source ($\bar{x} = 0$) is given by $\hat{u} = A(y) \sin (t)$, (29) must be solved subject to the following conditions:

$$t = 0, \quad p_1 = p_{1t} = 0; \tag{59}$$

$$\bar{x} = 0, \quad p_{1\bar{x}} = -A(y) \cos (t); \qquad \bar{x} \to \infty, \quad p_1 = \text{finite}; \tag{60}$$

$$y = 0; 1, \quad p_{1y} = 0. \tag{61}$$

A solution procedure identical to that used to solve (32)–(35) can be employed to obtain

$$p_1 = \tilde{A}_0 \sin (t - \bar{x}) + \sum_{n=1}^{\infty} \tilde{A}_n I_n(t, \bar{x}) \cos (n\pi y), \quad \bar{x} \leqslant t, \tag{62}$$

where I_n is the same integral as defined in (50). The Fourier coefficients $\tilde{A}_0$ and $\tilde{A}_n$ are defined by

$$A(y) = \tilde{A}_0 + \sum_{n=1}^{\infty} \tilde{A}_n \cos (n\pi y). \tag{63}$$

Equation (62) consists of a propagating axial wave mode of constant amplitude $\tilde{A}_0$, and an infinite number of dispersive higher modes. Note that unlike the $O(M)$ higher modes due to refraction considered earlier, here the higher modes, generated directly by the acoustic source, are of the same order of magnitude as the fundamental mode. After sufficient time elapses, in the absence of resonance, the solution may again be expressed in the quasi-steady form,

$$p_1 = \tilde{A}_0 \sin (t - \bar{x}) + \sum_{n=1}^{N} \frac{\tilde{A}_n}{(1 - q_n^2)^{\frac{1}{2}}} \sin [t - (1 - q_n^2)^{\frac{1}{2}} \bar{x}] \cos (n\pi y)$$

$$+ \cos (t) \sum_{n=N+1}^{\infty} \frac{\tilde{A}_n}{(q_n^2 - 1)^{\frac{1}{2}}} \exp [-(q_n^2 - 1)^{\frac{1}{2}} \bar{x}] \cos (n\pi y). \tag{64}$$

As an example, the boundary disturbance $\hat{u}(x = 0) = y \sin (t)$ in a laminar mean flow field with bulk velocity $\tilde{U}_0 = \frac{2}{3}$, is considered. This bulk velocity corresponds to $U = 4y(1 - y)$, although the explicit form of $U(y)$ is not needed for the leading-order calculation. The maximum mean flow Mach number is assumed to be 0.1. Figure 9(a–d) exemplifies the characteristic acoustic pressure signals at $x = 2\pi$ ($x' = \lambda'$), under four different driving acoustic frequencies, as evaluated numerically from (62). In each part of the figure, the time variations of p_1 on both duct walls ($y = 0, 1$) and at the centreplane ($y = \frac{1}{2}$) are depicted. In figure 9(a) $\Omega = 2$, lower than the cutoff frequency for the first oblique propagated mode in the duct. The resulting wave field is basically an axial one. Thus the pressure signals at three different y-locations on
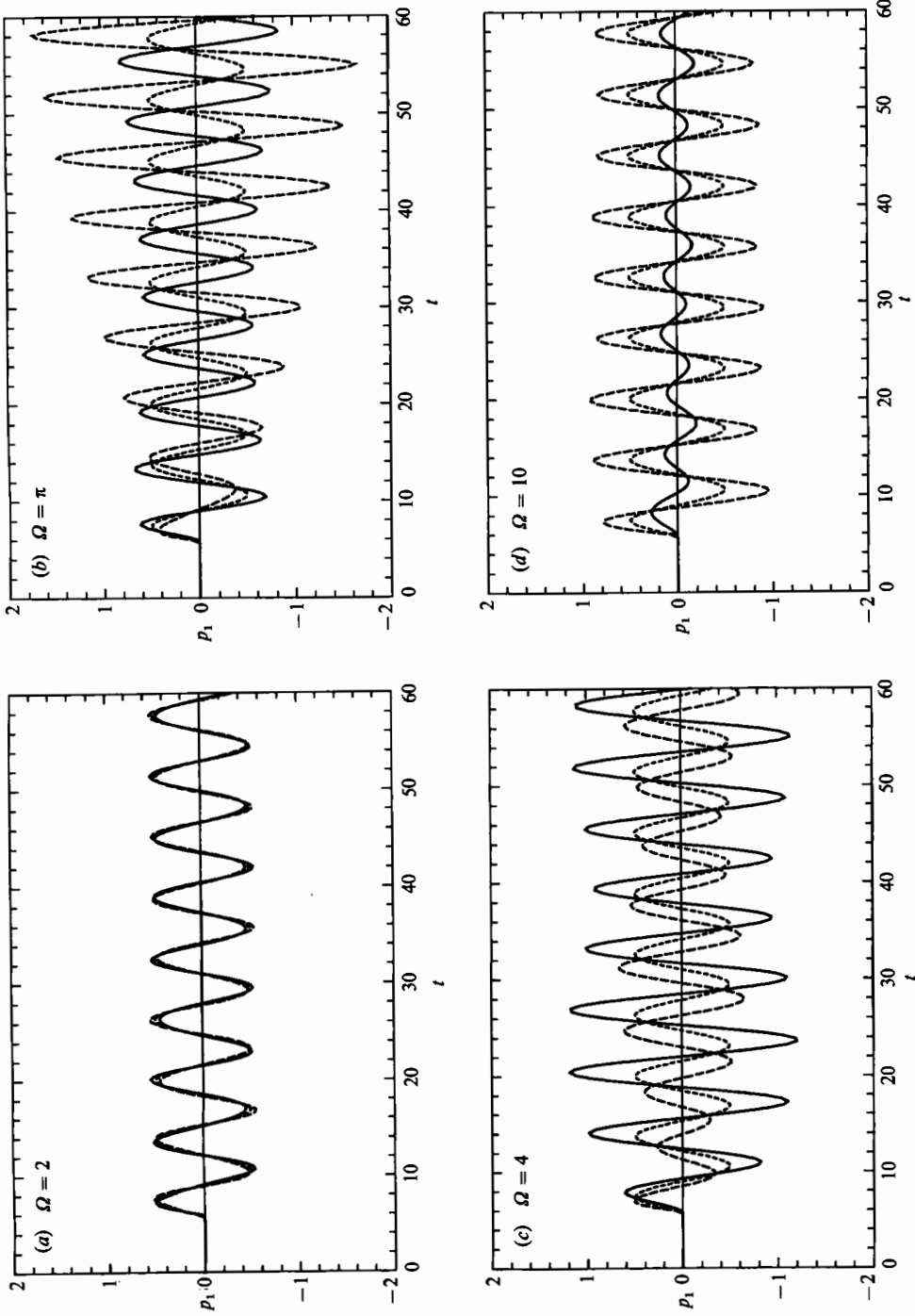
FIGURE 9. Time variations of the first-order acoustic pressure p_1 at three y-locations (——, $y = 0$; — — —, 1; ·····, $\frac{1}{2}$) on the duct cross-section $x = 2\pi$, as calculated from (62). The acoustic waves are generated by the y-dependent perturbation $\hat{u}(x = 0) = y \sin(t)$ in a mean flow field described by $U = 4y(1 - y)$, $M = 0.1$. The dimensionless frequencies are (a) $\Omega = 2$; (b) π; (c) 4; and (d) 10.

the same duct cross-section are almost the same, of amplitude approximately $\frac{1}{2}$ ($\tilde{A}_0$ in (63)). The small deviations are again attributed to the initial transients that diminish as time progresses. Figure 9(b) corresponds to $\Omega = \pi$, the resonant frequency for the first acoustic mode ($n = 1$), which causes p_1 to grow with time. The wave field is no longer purely axial because of the appearance of the transverse waves associated with the resonant mode. The results in figure 9(c) for $\Omega = 4$ contain both the fundamental mode and the first propagated oblique mode. The pressure curves vary with the y-coordinate but are bounded. Finally, in figure 9(d) the driving acoustic frequency is high enough to allow the third propagated oblique mode to appear in the duct, in addition to the fundamental and the first modes (note that the even modes do not appear because $A(y)$ is an odd function of y). The acoustic pressure curves differ dramatically from those in the previous three figures.

Additional numerical evaluations of p_1 show that when the acoustic frequency is varied within the range that allows a fixed number of propagated modes, the character of the wave field remains similar though the results vary in a quantitative sense. However, whenever the cutoff frequency of a new mode is crossed, there is a qualitative change in the wave phenomena.

The $O(M)$ refraction effect of this more general acoustic system could be studied by using the first-order results in (31). This is deferred to a future endeavour.

4. Acoustic boundary-layer solution

4.1. *Boundary-layer formulation*

In the acoustic boundary layer near the wall at $y = 0$, thermodynamic perturbations must be of the same order of magnitude as those found at the edge of the core flow. Therefore,

$$p = 1 + M^2 \gamma \tilde{p}, \quad \rho = 1 + M^2 \tilde{\rho}, \quad T = 1 + M^2 \tilde{T}, \tag{65}$$

where the tilde denotes acoustic quantities superimposed on the mean state. A stretched boundary-layer coordinate pointing away from the wall,

$$\eta = y/\delta, \tag{66}$$

is needed in order to describe the structure of the extremely slender acoustic boundary layer. A balance between diffusion and other important physical mechanisms in the general governing equations (2)–(6) can be obtained if

$$\delta = \left(\frac{M}{\Omega Re}\right)^{\frac{1}{2}}, \tag{67}$$

which provides the scale of the acoustic boundary-layer thickness. In dimensional terms, one finds the well-known result $\delta' \sim (\nu'/\omega')^{\frac{1}{2}}$, indicating explicitly the dependence of boundary-layer thickness upon the fluid viscosity and the frequency of the travelling acoustic waves. The appropriate scalings for fluid velocities in the layer, obtained by examining the asymptotic behaviour of (11) when $y \to 0$ for $\epsilon = M$, are given by

$$u = M\tilde{u} + \delta \eta U'(0) + \dots, \quad v = (M\delta) \tilde{v}. \tag{68}$$

The $O(\delta)$ contribution to u arises from the Taylor series expansion for $U(y)$ in the boundary layer, which is much smaller in magnitude than the horizontal acoustic velocity $M\tilde{u}$, given the assumption made in §2 that $M \gg 1/Re$. Consequently, the independent variable x, rather than $\bar{x}$, is an appropriate horizontal coordinate.

If the new dependent and independent variables defined in (65)–(68) are used, (2)–(6) can be transformed into

$$\gamma \tilde{p} - \tilde{\rho} - \tilde{T} = M^2 \tilde{\rho} \tilde{T}, \tag{69}$$

$$\tilde{\rho}_t + \tilde{u}_x + \tilde{v}_\eta = -M^2[(\tilde{\rho}\tilde{u})_x + (\tilde{\rho}\tilde{v})_\eta] + O(M\delta), \tag{70}$$

$$\tilde{u}_t - \tilde{u}_{\eta\eta} + \tilde{p}_x = -M^2(\tilde{\rho}\tilde{u}_t + \tilde{u}\tilde{u}_x + \tilde{v}\tilde{u}_\eta) + O(M^4) + O(M\delta), \tag{71}$$

$$\tilde{p}_\eta = O(\delta^2), \tag{72}$$

$$\tilde{T}_t - \frac{\gamma}{Pr}\tilde{T}_{\eta\eta} + (\gamma - 1)(\tilde{u}_x + \tilde{v}_\eta) = M^2\{\gamma(\gamma - 1)[\tilde{u}_\eta^2 - \tilde{p}(\tilde{u}_x + \tilde{v}_\eta)]$$
$$- (\tilde{\rho}\tilde{T}_t + \tilde{u}\tilde{T}_x + \tilde{v}\tilde{T}_\eta)\} + O(M^4) + O(M\delta). \tag{73}$$

The above equations are accurate representations of (2)–(6) in the acoustic boundary layer up to $O(M^2)$. The orders of magnitude of terms not written explicitly are indicated in each equation. It is interesting to notice that nonlinear product terms, which are responsible for acoustic streaming phenomena (Rott 1964), again turn out to be of $O(M^2)$ relative to leading-order acoustics. Terms of $O(M\delta)$ result from the residue mean flow velocity in the boundary layer (cf. (68)). These are higher-order small quantities, of size comparable with $O(M^4)$ terms under flow conditions described by, for example, $M = 0.1$ and $Re = 10^6$.

In the following solution development, correction terms of $O(M^2)$ and smaller in (69)–(73) are ignored. For convenience the same variable names (with an implicit zero subscript) will be used to describe the basic acoustic variations in the asymptotic series. Notice that although $O(M)$ terms do not appear in (69)–(73), the results are valid to $O(M)$, and are matched with the core solutions to the same order. The general matching conditions are expressed mathematically as

$$\Psi_{\text{b.l.}}(x, t, \eta \to \infty) \sim \Psi_{\text{core}}(x, t, y \to 0), \quad \Psi = (u, v, p, \rho, T). \tag{74}$$

On the duct wall the no-slip condition and the appropriate thermal conditions must be imposed.

4.2. Transient solutions

The acoustic pressure is seen from (72) to be basically uniform across the boundary layer, equal to that at the edge of the layer. Thus

$$\tilde{p} = \hat{p}(t, \bar{x}; y \to 0). \tag{75}$$

When the small correction terms on the right-hand side of (71) are truncated, the resulting equation, which describes the transient diffusion process of the horizontal velocity perturbation driven by the acoustic pressure, is seen to be decoupled from the others. It must be solved subject to the no-slip condition at $\eta = 0$. At $t = 0$, $\tilde{u}$ must vanish because there is no acoustic motion in the core. Following a standard Laplace transform procedure, the solution is obtained in integral form:

$$\tilde{u} = -\int_x^t \tilde{p}_x(\xi, \bar{x}) \, \text{erf}\left(\frac{\eta}{2(t-\xi)^{\frac{1}{2}}}\right) d\xi. \tag{76}$$

Equations (30), (46) and (62) can be used in (75) and (76) to evaluate the corresponding boundary-layer velocity.

It is also of interest to study the transverse acoustic velocity and other thermodynamic variables in the acoustic boundary layer. To this end (69), (70) and (73) are combined to find

$$\tilde{T}_t - \frac{1}{Pr}\tilde{T}_{\eta\eta} = (\gamma - 1)\tilde{p}_t, \tag{77}$$

which is a diffusion equation with a compressibility forcing function, valid to $O(M)$. An appropriate thermal condition needs to be specified at the duct wall, to obtain solutions for $\tilde{T}$ as well as $\tilde{\rho}$ and $\tilde{v}$. For simplicity two idealized types of thermal conditions, i.e. the adiabatic condition and the isothermal condition, are considered, with the understanding that practical situations usually lie in-between.

(i) *Adiabatic wall* $(\tilde{T}_\eta(\eta = 0) = 0)$. A formal solution to (77) subject to zero initial condition and the adiabatic wall condition yields the isentropic relations

$$\tilde{T} = (\gamma - 1)\tilde{p}, \quad \tilde{\rho} = \tilde{p} \tag{78}$$

if (69) is used. This indicates that no thermal diffusion exists, and all the thermodynamic quantities are uniform across the acoustic boundary layer. Equation (70) can be integrated to $O(M)$ by using (76) and (78) to give

$$\tilde{v} = -\tilde{p}_t\,\eta + \frac{\partial}{\partial x}\left[\int_{\bar{x}}^t \tilde{p}_x(\xi, \bar{x}) \int_0^\eta \mathrm{erf}\left(\frac{\zeta}{2(t-\xi)^{\frac{1}{2}}}\right)\mathrm{d}\zeta\,\mathrm{d}\xi\right], \tag{79}$$

which is zero on the wall surface. By employing integration by parts for the error function, the above result is rewritten as

$$\tilde{v} = \left[-\tilde{p}_t + \frac{1}{1+M\tilde{U}_0}\,\mathrm{erf}\left(\frac{\eta}{2(t-\bar{x})^{\frac{1}{2}}}\right) + \int_{\bar{x}}^t \tilde{p}_{xx}\,\mathrm{erf}\left(\frac{\eta}{2(t-\xi)^{\frac{1}{2}}}\right)\mathrm{d}\xi\right]\eta$$

$$+ \frac{1}{1+M\tilde{U}_0}\frac{2(t-\bar{x})^{\frac{1}{2}}}{\pi^{\frac{1}{2}}}\left(\exp\left[-\frac{\eta^2}{4(t-\bar{x})}\right] - 1\right) + \frac{2}{\pi^{\frac{1}{2}}}\int_{\bar{x}}^t \tilde{p}_{xx}(t-\xi)^{\frac{1}{2}}\left(\exp\left[-\frac{\eta^2}{4(t-\xi)}\right] - 1\right)\mathrm{d}\xi, \tag{80}$$

where the factor $1/(1+M\tilde{U}_0)$ arises from $\mathrm{d}\bar{x}/\mathrm{d}x$. Equation (80) is arranged according to terms that grow with η and those that remain $O(1)$ as $\eta \to \infty$. The former are driven by the refraction-induced transverse velocity in the core, and can be shown to match with the asymptotic behaviour of the corresponding core solution, given the coordinate transformation (66).

(ii) *Isothermal wall* $(\tilde{T}(\eta = 0) = 0)$. The mathematical system for $\tilde{T}$ is analogous to that for $\tilde{u}$. The solution can immediately be written down as

$$\tilde{T} = (\gamma - 1)\int_{\bar{x}}^t \tilde{p}_\xi(\xi, \bar{x})\,\mathrm{erf}\left(\frac{\eta_T}{2(t-\xi)^{\frac{1}{2}}}\right)\mathrm{d}\xi, \tag{81}$$

where

$$\eta_T = \eta(Pr)^{\frac{1}{2}} = \frac{y}{\delta_T} \tag{82}$$

is the vertical coordinate for the temperature boundary layer, of thickness characterized by $\delta_T = (M/(\Omega Pr Re))^{\frac{1}{2}}$. Equation (81) can be transformed into a more meaningful form by integrating the right-hand side by parts, and defining

$$\zeta = \frac{\eta_T}{2(t-\xi)^{\frac{1}{2}}}, \tag{83}$$

to give

$$\tilde{T} = (\gamma - 1)\left[\tilde{p}(t, \bar{x}) - \frac{2}{\pi^{\frac{1}{2}}}\int_{\frac{\eta_T}{2(t-x)^{\frac{1}{2}}}}^\infty \tilde{p}\left(t - \frac{\eta_T^2}{4\zeta^2}, \bar{x}\right)\mathrm{e}^{-\zeta^2}\,\mathrm{d}\zeta\right]. \tag{84}$$

The second term in the square brackets in (84), arising from conduction effects, describes the deviation in temperature from the isentropic condition represented by

$\tilde{p}(t, \bar{x})$. One notices that at $\bar{x} = t$, the instantaneous location of the acoustic wavefront in the core, both $\tilde{p}$ and $\tilde{T}$ are zero to match those quantities in the undisturbed flow field. The acoustic density and transverse velocity for the present case can be derived from (69) and (70), respectively. They are omitted here for brevity.

4.3. *Quasi-steady solutions*

As shown previously, core solutions for a non-resonant acoustic system as $t - \bar{x}$ becomes large consist of quasi-steady modes only. The corresponding boundary-layer solutions are more easily derived by using the complex notation. The acoustic pressure is written as a summation of complex Fourier series,

$$\tilde{p}(t, \bar{x}) = i \sum_{n=0}^{\infty} a_n \exp\left[-i(t - (1 - q_n^2)^{\frac{1}{2}}\bar{x})\right]. \tag{85}$$

Given (75), a comparison of (85) with the core pressure expressions shows that

$$a_0 = 1 - M \sum_{k=1}^{\infty} \frac{2\tilde{U}_k}{q_k^2},$$

$$a_n = M \frac{\tilde{U}_n(2 - q_n^2)}{q_n^2(1 - q_n^2)^{\frac{1}{2}}}, \quad n = 1, 2, \ldots \tag{86}$$

for the axial wave refraction case (cf. (30) and (52)), and

$$a_0 = \tilde{A}_0,$$

$$a_n = \frac{\tilde{A}_n}{(1 - q_n^2)^{\frac{1}{2}}}, \quad n = 1, 2, \ldots \tag{87}$$

for the non-axial wave case examined in §3.3 (cf. (64)), without considering the refraction effect.

The velocities in the acoustic boundary layer are dependent upon the boundary coordinate η. One can assume that the quasi-steady solution for each horizontal velocity mode is of the form $\tilde{u}_n = b_n(\eta) \exp\left[-i(t - (1 - q_n^2)^{\frac{1}{2}}\bar{x})\right]$. If this expression is substituted into (71) with (85), and the conditions $\tilde{u}_n(\eta = 0) = 0$; $\tilde{u}_n(\eta \to \infty) = O(1)$ are invoked, then the desired solution is

$$\tilde{u} = \sum_{n=0}^{\infty} \tilde{u}_n = \frac{i}{1 + M\tilde{U}_0} \sum_{n=0}^{\infty} a_n(1 - q_n^2)^{\frac{1}{2}} \left(1 - \exp\left(-\frac{1-i}{\sqrt{2}}\eta\right)\right) \exp\left[-i(t - (1 - q_n^2)^{\frac{1}{2}}\bar{x})\right], \tag{88}$$

where a_n is given by (86) or (87), depending on the core acoustic solutions. Equation (88) can be rewritten in terms of its real part, which is, for the refraction case,

$$\tilde{u} = \frac{1}{1 + M\tilde{U}_0} \left\{ \left(1 - M \sum_{k=1}^{\infty} \frac{2\tilde{U}_k}{q_k^2}\right) \left[\sin(t - \bar{x}) - \exp\left(-\frac{\eta}{\sqrt{2}}\right) \sin\left(t - \bar{x} - \frac{\eta}{\sqrt{2}}\right)\right] \right.$$

$$+ M \sum_{n=1}^{N} \tilde{U}_n \left(\frac{2}{q_n^2} - 1\right) \left[\sin(t - (1 - q_n^2)^{\frac{1}{2}}\bar{x}) - \exp\left(-\frac{\eta}{\sqrt{2}}\right) \sin\left(t - (1 - q_n^2)^{\frac{1}{2}}\bar{x} - \frac{\eta}{\sqrt{2}}\right)\right]$$

$$\left. + M \sum_{n=N+1}^{\infty} \tilde{U}_n \left(\frac{2}{q_n^2} - 1\right) \exp\left[-(q_n^2 - 1)^{\frac{1}{2}}\bar{x}\right] \left[\sin(t) - \exp\left(-\frac{\eta}{\sqrt{2}}\right) \sin\left(t - \frac{\eta}{\sqrt{2}}\right)\right] \right\}. \tag{89}$$

As the value of η increases, the η-dependent terms in (89) diminish exponentially, and the result is that of the inviscid core evaluated at $y = 0$.

The first term inside the curly braces in (89) is associated with the fundamental propagated mode in the core. It is the axial travelling wave counterpart of the classical Stokes solution (Stokes 1851). Thus the characteristic behaviour of the Stokes solution, including velocity overshoot (Richardson's annular effect) near the edge of the layer, and strong viscous damping near the wall will be observed (cf. figure 10). The amplitude of the fundamental mode deviates by $O(M)$ from unity, owing to the acoustic refraction effect (the infinite summation in the parentheses) and the bulk convection $(M\tilde{U}_0)$ caused by the mean shear flow in the core. In the case of downstream propagation the former effect augments the axial wave amplitude, while the latter damps it. For upstream wave propagation the reversed trend is obtained. Equation (89) also shows that the N higher propagated modes behave in the same way as the fundamental mode, except for decreased amplitude and increased phase speed as the mode number n increases. Each mode exhibits Richardson's annular effect, followed by smooth transition to no-slip velocity on the wall. Like the core solution, the effect of attenuated modes is limited to a region close to the acoustic source.

The result given by (89) is illustrated graphically in figures 10(a) and 10(b), which depict horizontal velocity profiles across the acoustic boundary layer when $\Omega = 2$ and 7 respectively, for $\frac{1}{4}\pi$ intervals over one acoustic period, at a location one-and-half wavelengths ($x = 3\pi$) downstream of the plane acoustic source. This location is sufficiently far from the acoustic source that the effects of stationary modes (last summation term in (89)) are virtually non-existent. The solid lines denote the horizontal velocity $\tilde{u}$ when a mean flow field, described by $U = 4y(1-y)$ and $M = 0.1$, is present in the core region. The velocity distributions for the case of no mean flow ($M = 0$), which corresponds to the Stokes solution, are also plotted as dashed lines for comparison. It is observed that when $\Omega = 2$, the analogous solid and dashed curves differ only by a constant multiplication factor (cf. (89)), because the only propagated mode in the duct is purely axial. The velocity amplitude is smaller than that of the Stokes solution due to the bulk convection, whose damping effect exceeds the amplifying effect of refraction at this low frequency. It should be pointed out that the pairs of solid and dashed curves in figure 10 are plotted at the same relative phase within a cycle beginning at their respective maximum velocity. The two solutions are out of phase in the absolute sense because the acoustic wave carried by the mean flow arrives at the given position sooner than that in the static field.

As the driving acoustic frequency becomes higher, the increased refraction amplifies the velocity oscillation. When $\Omega \approx 6$, the refraction effect roughly balances the bulk convection effect, and the velocity curves are found to coincide with those derived from the Stokes solution. The acoustic system remains dominated by the single fundamental mode until $\Omega \geqslant 2\pi$, when the second mode ($n = 2$) appears. Figure 10(b) depicts such a case where $\Omega = 7$. Here the amplitude of the acoustic velocity is larger than that of the Stokes velocity. The velocity profiles can no longer be obtained by multiplying the corresponding Stokes velocity profiles by a constant, because the addition of the second propagated mode alters the phase of the velocity at each time instant. Additionally, this mode makes the magnitudes of the velocity as well as pressure x-dependent because the oblique waves strike the boundary layer non-uniformly along its course of propagation (cf. figure 2).

On the acoustic source plane, $x = 0$, it can be shown that (89) takes the form

$$\tilde{u}(\bar{x} = 0) = \sin(t) - \exp\left(-\frac{\eta}{\sqrt{2}}\right)\sin\left(t - \frac{\eta}{\sqrt{2}}\right). \tag{90}$$
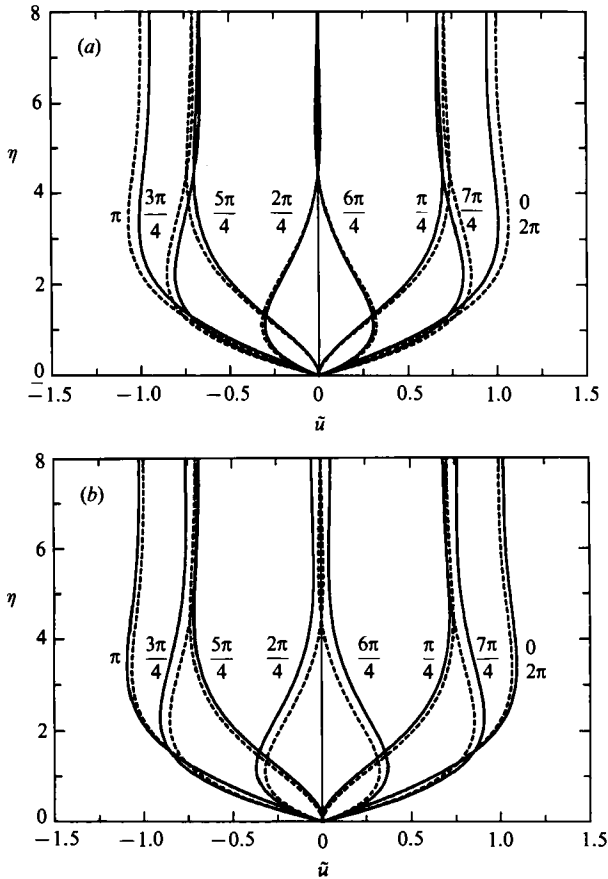
FIGURE 10. Profiles of quasi-steady horizontal velocity across the acoustic boundary layer at $x = 3\pi$, for $\frac{1}{4}\pi$ intervals over one acoustic period, when the mean flow in the core is described by $U = 4y(1-y)$ and $M = 0.1$, and the acoustic disturbance is $\hat{u}(x=0) = \sin(t)$. The dashed lines correspond to the Stokes solution ($M = 0$). The dimensionless frequencies are (a) $\Omega = 2$; (b) $\Omega = 7$.

All the $O(M)$ terms disappear because acoustic convection and refraction only take place away from the acoustic source. However, (90) does not satisfy the boundary condition (17) because non-zero $\tilde{v}$ is allowed at $x = 0$. A boundary-layer type of treatment which eliminates the slip velocity along the acoustic source plane will be necessary in order for the extra term in (90) to vanish.

The acoustic temperature and transverse velocity in the quasi-steady state depend on the thermal boundary condition along the duct wall. If the wall is adiabatic, the thermodynamic properties of the boundary-layer gas again obey the isentropic relation (78), and the transverse acoustic velocity is integrated from (70) to give

$$\tilde{v} = \sum_{n=0}^{\infty} a_n \left\{ \left[\frac{1-q_n^2}{(1+M\tilde{U}_0)^2} - 1 \right] \eta \right.$$

$$\left. + \frac{1-q_n^2}{(1+M\tilde{U}_0)^2} \frac{1+\mathrm{i}}{\sqrt{2}} \left(\exp\left(-\frac{1-\mathrm{i}}{\sqrt{2}} \eta \right) - 1 \right) \right\} \exp\left[-\mathrm{i}(t - (1-q_n^2)^{\frac{1}{2}} x) \right]. \quad (91)$$
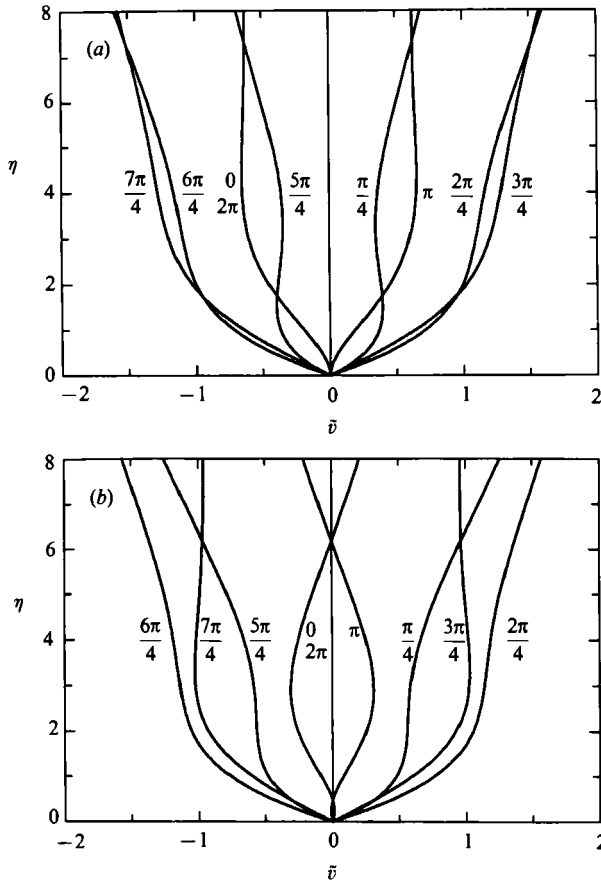
FIGURE 11. Profiles of quasi-steady transverse velocity across the acoustic boundary layer adjacent to an adiabatic duct wall, at $x = 3\pi$, for $\frac{1}{4}\pi$ intervals over one acoustic period, under conditions identical to those in figure 10. The dimensionless frequencies are (a) $\Omega = 2$; (b) $\Omega = 7$.

Figures 11(a) and 11(b) display the transverse velocity profiles, calculated from (91), under conditions identical to those employed in figures 10(a) and 10(b) respectively. The transverse boundary-layer motion for $\Omega = 7$ is quite different from that for $\Omega = 2$, owing to the existence of the oblique acoustic waves in the core in the former case. As η becomes large, both cases exhibit growth in velocity amplitude with η to match with that in the core, in contrast to the transverse velocity in a Stokes boundary layer whose amplitude approaches a constant as the edge of the layer is approached.

If the wall is kept at constant temperature, the solution for $\tilde{T}$ and $\tilde{v}$ can be derived from (77) and (70) in the same manner. They are expressed below in the complex form:

$$\tilde{T} = \mathrm{i}(\gamma - 1) \sum_{n=0}^{\infty} a_n \left(1 - \exp\left(-\frac{1-\mathrm{i}}{\sqrt{2}}\eta_T\right)\right) \exp\left[-\mathrm{i}(t - (1 - q_n^2)^{\frac{1}{2}}\bar{x})\right], \qquad (92)$$

$$\tilde{v} = \sum_{n=0}^{\infty} a_n \left\{\left[\frac{1-q_n^2}{(1+M\tilde{U}_0)^2} - 1\right]\eta + \frac{1-q_n^2}{(1+M\tilde{U}_0)^2}\frac{1+\mathrm{i}}{\sqrt{2}}\left(\exp\left(-\frac{1-\mathrm{i}}{\sqrt{2}}\eta\right) - 1\right)\right.$$

$$\left. + \frac{\gamma-1}{(Pr)^{\frac{1}{2}}}\frac{1+\mathrm{i}}{\sqrt{2}}\left(\exp\left(-\frac{1-\mathrm{i}}{\sqrt{2}}\eta_T\right) - 1\right)\right\} \exp\left[-\mathrm{i}(t - (1 - q_n^2)^{\frac{1}{2}}\bar{x})\right]. \quad (93)$$

The similar forms of (92) and (88) suggest that in the thermal boundary layer adjacent to an isothermal wall, the temperature diffuses in the same way as the horizontal velocity does in the viscous boundary layer. The first two terms in the curly braces of (93) are identical to those in (91), representing the effect of momentum diffusion driven by the acoustic waves in the core. In addition, thermal expansion of the gas due to non-uniform temperature distribution across the layer also contributes to the transverse fluid motion. This effect is represented by the last term in the curly braces of (93).

The fundamental mode in (92) and (93) can be shown to agree with the results obtained by Rott (1980) where the effect of the mean shear flow is removed. An important contribution of the mean shear flow is to generate a variety of acoustic waves that all contribute to the larger transverse velocity, represented in the acoustic boundary layer by the term proportional to η in (91) and (93). In the limit $\eta \to \infty$, the magnitude of this term exceeds that of all the others, thus (91) and (93) have the same asymptotic behaviour which can be shown to match with that of the core solution.

5. Discussion and conclusions

In this study a systematic analysis has been developed to discover the effect of a low-Mach-number shear flow on acoustic wave propagation in a planar duct. Two distinct flow regions are considered: the inviscid, non-heat-conducting core region and the thin acoustic boundary layer near the wall of the duct. The mathematical analysis is carried out in the limit $M \to 0$ for $Re \gg O(1/M)$, when the axial wavelength is longer than or comparable (in the order of magnitude sense) with the duct width.

Solutions for the acoustic pressure and velocity describe both short-time acoustic transients and long-time evolution for both non-resonant and resonant cases. This study bridges the recent transient numerical study of Baum & Levine (1987) and earlier quasi-steady studies (Pridmore-Brown 1958, for example) and, more importantly, provides new results not available in those investigations. More physical insights into the refraction mechanism are obtained by demonstrating explicitly the interactions between the mean flow and the various types of acoustic waves represented by Fourier modes whose summation describes the global variations in acoustic quantities.

It is of interest to compare the present perturbation results with the numerical solutions of Baum & Levine (1987), to shed light on a number of issues raised in their initial-boundary-value numerical study valid over a few acoustic periods.

(i) *Acoustic refraction magnitude.* The following examples are used to demonstrate that the present linear analysis yields refraction magnitudes comparable with those from numerical solutions to the Navier–Stokes equations (Baum & Levine 1987). In a duct of width $d' = 0.1$ m, with a symmetric mean flow described by the one-seventh power law, a centreplane Mach number $M = 0.1$ and sound speed $c' = 340$ m/s, the dimensionless frequency corresponding to $f' = 3000$ Hz is $\Omega \approx 2.772$, less than the cutoff frequency for the first oblique wave. The quasi-steady axial wave solution is thus representative of the acoustic refraction phenomena since the transient effects are relatively small. The pressure amplitude near the wall, as calculated from (55), is 4.5% larger than that at the centreplane. This result compares well with the numerical result of 6.4% by Baum & Levine (1987), who employed the same conditions except that d' is the diameter of an infinite cylinder. When the acoustic

frequency is changed to 1000 Hz ($\Omega = 0.924$), the linear asymptotic solution and nonlinear numerical solution yield near-wall acoustic pressure increases of 0.50 % and 0.55 % respectively, relative to the centreline pressures. They are again in good agreement. The above comparisons should of course be interpreted in the qualitative sense, in view of the different geometries (parallel duct *vs.* circular cylinder) and flow models (laminar *vs.* turbulent k–ϵ model) used in the two studies. Nonetheless they demonstrate that linear studies can predict refraction effects accurately, and that the two types of solutions are in qualitative agreement if comparisons are made in the same parameter range. In the light of these conclusions, it is likely that the differences between linear and nonlinear results noted by Baum & Levine (1987) result from comparisons in inappropriate parameter regimes.

(ii) *Acoustic boundary-layer thickness and structure.* The boundary-layer structure described in the perturbation solution, including the Richardson's annular effect and the substantial viscous damping, also agrees qualitatively with that found by Baum & Levine (1987). In particular, it is of interest to compare the boundary-layer thickness predicted by the analysis with that from the numerical work.

The effective thickness of the velocity boundary layer, as defined by Lighthill (1978), is given by $5\delta = 5(M/(\Omega Re))^{\frac{1}{2}}$. According to figure 10, this corresponds to the distance away from the solid wall at which the amplitude of $\tilde{u}$, after the overshoot, approaches its asymptote of constant value to within approximately 2.7 %. For acoustic waves of frequency 1000 Hz travelling in air contained within a duct of width 0.1 m, under standard conditions (one atmospheric pressure and room temperature), the calculated boundary-layer thickness is approximately 0.25 % the width of the duct. This result should also hold for wave motion in a circular cylinder of diameter equal to the duct width, because the curvature effect is negligible in the extremely thin layer. If the same criterion of 2.7 % deviation is applied to figure 14 of Baum & Levine (1987), one finds a boundary-layer thickness of approximately 0.35 % of the diameter of the cylinder. This result is actually larger than, but agrees well in the order of magnitude sense with, the linear perturbation prediction. Similar agreement is observed in terms of the maximum velocity overshoots and the locations where they occur. Thus we do not agree with the conclusion of Baum & Levine (1987) that linear theory significantly overpredicts the boundary-layer thickness.

(iii) *Nonlinear effect and acoustic streaming.* In the present work, through a systematic rational approximation and perturbation procedure, it has been demonstrated in (13)–(15) that the convective nonlinear terms are $O(M)$ smaller than those responsible for acoustic refraction when $x = O(1)$. Although the former can have an accumulative effect which eventually leads to waveform deformation and weak shock formation, the nonlinearization process becomes prominent only after the wave travels a distance of $x = O(M^{-2})$ (Kevorkian & Cole 1981; Wang & Kassoy 1990). Nonlinearity cannot have a profound influence on either the acoustic or the overall flow quantities, on the $O(1)$ time and length scales considered by Baum & Levine (1987). In the acoustic boundary layer the nonlinear terms are again shown to be $O(M^2)$ relative to the basic variations occurring there (cf. (69)–(73)). Acoustic streaming associated with the nonlinear convective terms is thus insignificant relative to the amplitude of refraction effects. The relatively good agreements between the present fundamentally linear solutions and the fully nonlinear numerical solutions in terms of refraction size and acoustic boundary-layer structure, discussed above, also attest to the insignificance of the nonlinear phenomena.

The major findings of the present study can be summarized as follows. When a

plane acoustic source of uniform strength is placed across a duct containing an undisturbed shear flow, it induces leading-order purely axial and quasi-steady acoustic waves propagating at a speed which is modified by $O(M)$ due to bulk convection. Second-order acoustic quantities, including y-dependent axial and oblique propagating waves, as well as bulk forced oscillations that affect only a narrow region near the plane acoustic source, are generated as a result of leading-order axial wave refraction by the mean flow velocity gradient. The propagated and attenuated wave modes exhibit transient phenomena initially, and evolve gradually, in the absence of resonance, into their respective quasi-steady state long after the passage of the axial wavefront.

Resonance occurs when the duct width is an integer multiple of the driving acoustic wavelength. Then, the refraction of the axial wave induces an amplifying purely transverse wave. In general, the refraction effect increases with the driving frequency as well as the mean flow Mach number, and decreases with the wave amplitude. The refraction-induced $O(M)$ wave phenomena become increasingly complex as the number of propagated modes, which is proportional to the driving frequency for given duct geometry, increases. At low frequency, when the driving acoustic wavelength is greater than the duct width, the only propagating waves are axial, and the net effect of acoustic refraction is to distort the pressure distribution across the wave by $O(M)$. The quasi-steady solutions agree with the classical axial wave solutions.

In the thin acoustic boundary layer, typically with thickness of less than 1 % of the duct width, the acoustic pressure is basically uniform across the layer, equal to that at the outer edge of the layer. The boundary layer responds to all the acoustic modes existing in the core region, generating complex velocity and temperature responses. Quasi-steady solutions again exist when resonance is absent, after an initial transient period. The horizontal velocity component for each acoustic mode exhibits Richardson's annular effect, followed by smooth transition to a no-slip boundary condition on the wall. The total horizontal velocity deviates by $O(M)$ from the Stokes solution, because of the acoustic refraction and convection effects generated in the core. The transverse velocity grows with the transverse boundary-layer coordinate, and is matched by the core solution outside the layer.

REFERENCES

BARNETT, D. O. 1970 An analytical investigation of heat transfer in pulsating turbulent flow in a tube. Ph.D. dissertation, Auburn University.

BARNETT, D. O. 1981 The effect of pressure pulsations and vibrations in fully developed pipe flow. *Re.* AEDC-TR-80-31. Arnold Engineering Development Center.

BAUM, J. D. & LEVINE, J. N. 1987 Numerical investigation of acoustic refraction. *AIAA J.* **25**, 1577–1586.

GRADSHTEYN, I. S. & RYZHIK, I. M. 1980 *Table of Integrals, Series, and Products*, Corrected and Enlarged Edn. Academic.

HERSH, A. S. & CATTON, I. 1971 Effect of shear flow on sound propagation in rectangular ducts. *J. Acoust. Soc. Am.* **50**, 992–1003.

KEVORKIAN, J. & COLE, J. D. 1981 *Perturbation Methods in Applied Mathematics*. Springer.

LIGHTHILL, M. J. 1978 Acoustic streaming. *J. Sound Vib.* **61**, 391–418.

MORSE, P. M. & INGARD, K. U. 1968 *Theoretical Acoustics*. McGraw-Hill.

MUNGUR, P. & GLADWELL, G. M. L. 1969 Acoustic wave propagation in a sheared fluid contained in a duct. *J. Sound Vib.* **9**, 28–48.

OBERHETTINGER, F. & BADII, L. 1973 *Tables of Laplace Transforms*. Springer.

PRIDMORE-BROWN, D. C. 1958 Sound propagation in a fluid flowing through an attenuating duct. *J. Fluid Mech.* **4**, 393–406.

RICHARDSON, E. G. & TYLER, E. 1929 The transverse velocity gradient near the mouths of pipes in which an alternating or continuous flow of air is established. *Proc. Phys. Soc. Lond.* **42**, 1–15.

ROMIE, F. E. 1956 Heat transfer to fluids flowing with velocity pulsations in a pipe. Ph.D. dissertation, University of California, Los Angeles.

ROTT, N. 1964 Theory of time-dependent laminar flows. In *High Speed Aerodynamics and Jet Propulsion*, vol. IV, pp. 395–438. Princeton University Press.

ROTT, N. 1980 Thermoacoustics. *Adv. Appl. Mech.* **20**, 135–175.

SCHLICHTING, H. 1979 *Boundary Layer Theory*, Seventh Edn. McGraw-Hill.

SEXL, T. 1930 Annular effect in resonators observed by E. G. Richardson. *Z. Phys.* **61**, 349–362.

STOKES, G. G. 1851 On the effect of the internal friction of fluids on the motion of pendulums. *Trans. Camb. Phil. Soc.* **9**(II), 8–106.

UCHIDA, S. 1956 The pulsating viscous flow superposed on the steady laminar motion of incompressible fluid in a circular pipe. *Z. Angew. Math. Phys.* **7**, 403–422.

WANG, M. & KASSOY, D. R. 1990 Evolution of weakly nonlinear waves in a cylinder with a movable piston. *J. Fluid Mech.* **221**, 27–52.